https://doi.org/10.1016/j.ymssp.2019.05.037

Acoustical Coupling and Radiation Control of Open Cavity Using an Array of Helmholtz Resonators

Zhibo Wang and Yatsze Choy[1]

Department of Mechanical Engineering,

The Hong Kong Polytechnic University,

Kowloon, Hong Kong SAR, PR China

[1]Corresponding author email: mmyschoy@polyu.edu.hk

Abstract

This paper presents the theoretical and experimental investigations on the suppression of noise radiation from a point source inside an open cavity with three-dimensional configuration using several Helmholtz resonators (HRs). A theoretical model is established based on the modal superposition method to study the acoustical coupling between a rectangular open cavity and multiples HRs. Additionally, a baffled open cavity is considered to couple acoustically with a semi-infinite exterior field using the acoustic coupled mode theory. The theoretical model facilitates the understanding of the mechanism of the peak formation in the sound pressure level spectrum at the receiving points outside the cavity and the noise suppression mechanism by the HRs. In addition, the relationship between those sound peaks, and that of the resonances of the enclosed cavity and open cavity are investigated to have a good design of HR. The location and internal resistance of HR are optimised to obtain a desirable attenuation of noise radiation from the open cavity. Subsequently, experiments are performed to validate the proposed model and examine the feasibility of the HR in suppressing noise radiation from the open cavity. The noise reduction around the sound peak indicates that both the single and multiple sound peaks of the open cavity can be controlled successfully by adopting HRs. The practical significance of this study is to provide a new insight into sound reduction in an open acoustical system through suppressing the resonant response by resonators.

Keywords: noise radiation control, open cavity, Helmholtz resonator

1. Introduction

An open cavity can be found in many applications such as parallel acoustic barriers, computer enclosures installed with rotating fans, and solid propellant boosters for submarines. Noise is generated by a sound source inside the cavity and is radiated to an infinite space through the cavity opening. Sound generated inside the cavity does not dissipate but, rather, reverberates within the structure. The noise emitted from the open cavity is likely to disturb humans nearby. Many approaches, either analytical or numerical, have been conducted on the theoretical investigation and analysis of the sound field inside and outside the cavity [1-15]. For example, Tam [1] studied the acoustic modes of a two-dimensional open rectangular cavity theoretically and established a semi-analytical formula to determine the natural frequencies of the rectangular open cavity in a no-flow situation. Wang et al.[2] and Kim et al. [4] investigated the sound radiation from an opening in a rectangular enclosure, and analysed the sound field in an outdoor space. The sound pressure outside a cavity was calculated using the Kirchhoff–Helmholtz integral while the sound pressure inside the cavity was solved by the modal superposition method. Apart from the analytical investigations, numerical methods such as the boundary element method (BEM) and finite element method (FEM) can provide the solutions for the problem of open cavity with different geometries. Yang et al. [7] found the acoustic resonances of the open cavity bounded by parallel barriers using the FEM with a perfect matched layer (PML) [16]. The BEM was used by Seybert et al. [11] to obtain the solution of coupled interior/exterior acoustic problems. To maintain the advantages of numerical methods and improve the computational efficiency, hybrid methods have been used widely to couple the acoustic fields in the interior and exterior regions, and they have been proven to be highly efficient and accurate in solving acoustic radiations from a cavity with an unbaffled plane [13-15] or complex geometry [14]. The previous studies showed that multiple sound peaks were obtained at the receiving point outside the open cavity. The corresponding frequencies of these peaks were near the resonances of the cavity and closely related to the enclosed-cavity modes [2]. At these frequencies, sound pressure distribution inside the cavity appear in the

acoustic modal patterns. The radiation at the cavity opening causes the sound pressure distribution to deviate from the fully enclosed-cavity modes [7]. Outside the cavity, the sound pressure decreases with distance. Such sound pressure distribution are almost the same as the trapped modes in an open cavity. Trapped modes, which are also referred to as resonance modes or bound states, are time-harmonic solutions of the homogeneous Helmholtz equation with local geometrical or material variations [17]. A unique characteristic of the trapped mode for the open cavity is that most of its acoustical energy is trapped in a local area, and the energy density outside decays with distance [7]. Trapped modes have been identified in many open acoustic systems, such as open channels [18], pipes and tunnels [19], ducted cavities [20-22], and waveguides [23-25]. Yang et al. [7] used the trapped modes to calculate the sound response at the receiver behind the parallel barriers in order to understand the acoustic modal contributions. However, the sound pressure agreement can only be found at the resonance frequencies when comparing with that calculated by BEM and there is large divergences at off resonance frequencies. To solve this problem, Recently, Tong et al. [14] presented the sound field of an open cavity based on the acoustic coupled mode theory. In their method, the sound field inside the cavity is calculated by using acoustic coupled mode theory. However, the acoustic interaction between outside sound field and acoustic mode inside the open cavity are not well studied.

The aforesaid studies were primarily devoted to the theoretical modelling of sound fields inside and outside the open cavity. However, studies regarding the noise radiation control of open cavity are limited. Recently, Wang et al. [2, 26-28] developed an active noise control system, named planar virtual sound barrier that consists of microphones, loudspeakers, and control circuits at the opening of the baffled rectangular cavity. A high noise reduction near the resonant frequencies of the open cavity was observed. Although an active method can offer a solution for the sound radiation suppression from the open cavity, this method was hardly applied widely owing to excessive expenditures and complicated counterparts. For the passive noise control approach, Ortiz et al. [29] adopted microperforated panels (MPPs) to attenuate resonant peaks radiating from an open cavity. However,

the mechanism regarding the acoustical coupling between the MPP absorber and open cavity was not explained. Up to now, little attention is devoted on the study of passive noise control of sound radiation from an open cavity. To reduce the peaks of the sound pressure level spectrum at the point outside the open cavity, one or multiple Helmholtz resonators (HRs) have been proposed to be mounted on the walls of the open cavity to distort the formation of resonance of the open cavity. Preliminary studies on parallel acoustic barriers indicated that an HR can distort the sound pressure distribution between parallel barriers [30]. Additionally, although HRs have been used extensively in ducts [31-33] and enclosure systems [34-37], the acoustic interference between an HR and open cavity of a three-dimensional configuration, and the suppression mechanism of sound radiation from a cavity opening to an infinite space have not been investigated.

Therefore, the objectives of the current study are (1) to obtain a general solution for the acoustical coupling between an HR and three-dimensional open cavity to predict the coupled sound pressure field inside and outside the open cavity; (2) to conduct eigenvalue analysis on the coupled system and obtain the relationship among the resonance frequencies of an enclosed cavity mode, open cavity trapped mode, and sound pressure level peak. This is because previous works [1, 2, 14, 22] have demonstrated that the frequencies of the sound peaks are higher than the resonant frequencies of the enclosed cavity modes; (3) to study the effect of position and internal resistance of an HR, and to optimise their properties such that the desirable acoustic performance can be obtained.

In this study, an HR is developed and mounted on the cavity wall to suppress noise radiation from the cavity opening to the infinite space outside. The theoretical model of acoustical coupling of a baffled open cavity and HR array is established. The mechanism of the resonator for noise radiation control is verified, and the effects of natural frequency, location, and internal resistance of the resonator on noise reduction performance are discussed. Finally, an experiment is conducted to validate the theoretical model and demonstrate the feasibility of using HRs to control noise radiation from an open acoustic system.

2. Theoretical formulations

2.1 Description of the model

Figure 1 shows a model of a rectangular cavity with an opening placed on an infinite baffle and a classical HR mounted on a wall. The open cavity considered in the current study can be found widely in architectural acoustics and engineering occasions. A Cartesian coordinate system is adopted where the origin is fixed at the upper left corner vertex of the cavity. The cavity consists of five acoustically rigid walls of dimensions L_x, L_y, and L_z in the x, y, and z directions, respectively. The classical HR consists of a narrow neck and a backing cavity. A rigid acoustic baffle is fixed at $z = 0$ and on the x-y plane. The entire space of the open cavity is divided into the cavity region Ω_a and an upper-half semi-infinite region Ω_b through the cavity opening S_{op}. Such an acoustical open system is excited by a primary sound source inside the cavity.

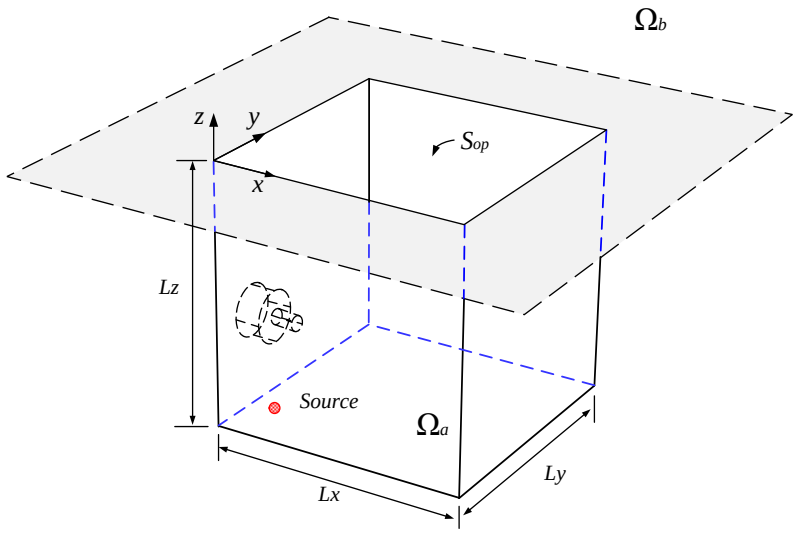

Figure 1 The sketch of baffled open cavity coupled with a Helmholtz resonator.

Omitting the time dependence $e^{i\omega t}$, the sound pressure p_a inside the baffled open cavity can be obtained by the three-dimensional inhomogeneous Helmholtz equation:

$$\nabla^2 p_a(\boldsymbol{x}) + k^2 p_a(\boldsymbol{x}) = -Q_s \delta(\boldsymbol{x} - \boldsymbol{x}_s), \tag{1}$$

where k is the wavenumber; ω is the angular frequency; Q_s and $\boldsymbol{x}_s = (x_s, y_s, z_s)$ are the strength and location of the primary sound source, respectively; δ is the Dirac delta function and ∇ is the Laplace

operator.

Further, the corresponding sound pressure p_b outside the baffled open cavity is obtained by the homogenous Helmholtz equation:

$$\nabla^2 p_b(\boldsymbol{x}) + k^2 p_b(\boldsymbol{x}) = 0, \tag{2}$$

On the cavity wall surface and the opening, we have

$$\frac{\partial p_a}{\partial n} = \begin{cases} -i\rho k c v_n & \text{on cavity opening } S_{\text{op}} \\ 0 & \text{on rigid wall surface} \end{cases}, \tag{3}$$

where n denotes the outer normal direction of the cavity surface; ρ and c are the mass density and sound speed of the medium in the cavity, respectively; v_n is the normal particle velocity at the cavity opening according to the momentum equilibrium.

Assuming that the largest dimension of the resonator aperture is smaller than the sound wavelength of interest, the volume velocity source strength density out of the Helmholtz resonator can be computed as follows:

$$\left.\frac{\partial p_a}{\partial n}\right|_{\boldsymbol{x}_t^R} = -i\rho k c \frac{p_a \delta\left(\boldsymbol{x} - \boldsymbol{x}_t^R\right)}{Z_t^R}, \tag{4}$$

Z_t^R is the output impedance at the t^{th} resonator's mouth located at $\boldsymbol{x}_t^R$. It is noteworthy that the signs of the volume velocity from the resonators are the same as that of the primary sound source, indicating that the sound is radiated into the cavity.

The boundary condition for the rigid baffle is

$$\left.\frac{\partial p_b}{\partial n}\right|_{z=0} = 0, \quad \left(x < 0, x > L_x \text{ and } y < 0, y > L_y\right). \tag{5}$$

According to the non-Hermitian Hamilton principle that was originally used in quantum mechanics [38, 39] and subsequently extended to solve the acoustical coupling in an open system [14, 24, 40], the sound property in acoustical open systems can be solved by relying on the spectral properties of their closed counterparts. Therefore, the sound pressure within the open cavity Ω_a is expanded as the

superposition of the closed-cavity modal function.

$$p_a(\boldsymbol{x}) = \sum_{l=0}^{\infty}\sum_{m=0}^{\infty}\sum_{n=0}^{\infty} a_{lmn}\phi_{lmn}(\boldsymbol{x}), \tag{6}$$

where a_{lmn} is the modal response of the eigenfunction $\phi_{lmn}(\boldsymbol{x})$; l, m, and n are the modal indices in the x, y, and z directions, respectively. $\phi_{lmn}(\boldsymbol{x})$ forms a complete, orthogonal basis set and is calculated by

$$\phi_{lmn}(\boldsymbol{x}) = \psi_l(x)\psi_m(y)\psi_n(z), \quad \psi_i(x) = \sqrt{\left(2-\delta_{0,i}\right)/L_i}\cos\left(i\pi x/L_i\right), \tag{7}$$

where $\delta_{i,j}$ is the Kronecker delta function.

The corresponding wave number of the eigenmodes $\phi_{lmn}(\boldsymbol{x})$ is

$$k_{lmn}^2 = \left(\frac{l\pi}{L_x}\right)^2 + \left(\frac{m\pi}{L_y}\right)^2 + \left(\frac{n\pi}{L_z}\right)^2. \tag{8}$$

From Rayleigh's integral [41], the sound pressure p_b in the outside region Ω_b owing to the vibration on the cavity opening could be written in an integral form as follows:

$$p_b(\boldsymbol{x}) = i\rho kc\int_{S_{op}} G\cdot v_n dS_{op}, \tag{9}$$

where $G = \frac{1}{2\pi}\frac{e^{-ikr}}{r}$; $r = \left|\boldsymbol{x}-\boldsymbol{x}_{op}\right|$ is the distance between the field point $\boldsymbol{x}$ and the opening point $\boldsymbol{x}_{op}$. The normal particle velocity v_n is expressed as follows:

$$v_n = \sum_{\mu=0}^{\infty}\sum_{\nu=0}^{\infty} b_{\mu\nu}\chi_{\mu\nu}\left(x_{op}, y_{op}\right), \tag{10}$$

where $\chi_{\mu\nu} = \psi_\mu(x)\cdot\psi_\nu(y)$ and $b_{\mu\nu}$ is the modal response of the ($\mu\nu$) mode. This is because $\{\psi_\mu(x)\cdot\psi_\nu(y),\ \mu,\ \nu = 0, 1, 2, \ldots\}$ forms a complete set of function, and therefore can be used to express the normal particle velocity distribution on the cavity opening S_{op} [13]. Similar treatments can be found in Xiong et al. [9], Tong et al. [13], and Wang and Choy [14].

Substituting Eq. (10) into Eq. (9), the sound pressure p_b in region Ω_b can be rewritten as

$$p_b(\boldsymbol{x}) = \sum_{\mu=0}^{\infty}\sum_{\nu=0}^{\infty} b_{\mu\nu}\varphi_{\mu\nu}(\boldsymbol{x}), \tag{11}$$

where the external mode $\varphi_{\mu\nu}(\boldsymbol{x})$ is expressed as [14]

$$\varphi_{\mu\nu}\left(\boldsymbol{x}\right)=i\rho kc\int_{S_{op}}G\chi_{\mu\nu}dS_{op}\,. \tag{12}$$

Thus far, the sound pressures p_a and p_b inside and outside the open cavity, respectively, have been expressed based on the enclosed-cavity modes and external modes, respectively. The modal coefficients a_{lmn} and $b_{\mu\nu}$ can be determined by the following procedure.

The second Green identity is first applied for the cavity space Ω_a and yields

$$\int_{\Omega_a}p\nabla^2\phi_i d\Omega_a-\int_{\Omega_a}\phi_i\nabla^2 p d\Omega_a+\int_S\phi_i\frac{\partial p}{\partial \boldsymbol{n}}ds-\int_S p\frac{\partial\phi_i}{\partial \boldsymbol{n}}ds=0\,. \tag{13}$$

In the equation above, the surface integral is evaluated on the entire surface of the cavity, including the openings of the cavity and resonators.

Using Eqs. (3), (4), (6)- (8), Eq. (13) is rewritten as

$$\begin{aligned}&\sum_{l=0}^{\infty}\sum_{m=0}^{\infty}\sum_{n=0}^{\infty}\left[a_{lmn}\left(k^2-k_{l'm'n'}^2\right)\int_{\Omega_a}\phi_{l'm'n'}\phi_{lmn}d\Omega_a\right]-i\rho kc\int_{s_{op}}\phi_{l'm'n'}v_n ds_{op}\\&=-i\rho kcq_s\phi_{l'm'n'}\left(\boldsymbol{x}_s\right)+\sum_{t=1}^{T}\frac{i\rho kc}{Z_t^R}\int_{s_R}\left[\phi_{l'm'n'}\sum_{l"=0}^{\infty}\sum_{m"=0}^{\infty}\sum_{n"=0}^{\infty}a_{l"m"n"}\phi_{l"m"n"}\delta\left(\boldsymbol{x}-\boldsymbol{x}_t^R\right)\right]ds_R\end{aligned}\,. \tag{14}$$

Equation (14) considers the interactions between the open cavity and multiple resonators, in which the effect of cavity opening on the acoustical coupling of the cavity–resonator system is indicated by the normal particle velocity v_n.

Substituting the modal expression of v_n and applying the orthogonal property of eigenmodes, Eq.(14) is simplified as

$$\begin{aligned}&a_{lmn}\left(k^2-k_{lmn}^2\right)-i\rho kc\sum_{\mu=0}^{\infty}\sum_{\nu=0}^{\infty}b_{\mu\nu}\int_{s_{op}}\phi_{lmn}\chi_{\mu\nu}ds_{op}\\&=-i\rho kcq_s\phi_{lmn}\left(\boldsymbol{x}_s\right)+\sum_{t=1}^{T}\frac{i\rho kc}{Z_t^R}\int_{s_R}\left[\phi_{lmn}\sum_{l"=0}^{\infty}\sum_{m"=0}^{\infty}\sum_{n"=0}^{\infty}a_{l"m"n"}\phi_{l"m"n"}\delta\left(\boldsymbol{x}-\boldsymbol{x}_t^R\right)\right]ds_R\end{aligned}\,. \tag{15}$$

Subsequently, the sound pressure continuity at the opening is considered such that

$$p_a\left(\boldsymbol{x}\right)\big|_{s_{op}}=p_b\left(\boldsymbol{x}\right)\big|_{s_{op}}\,. \tag{16}$$

Using Eqs (6) and (11), Eq. (16) is reshaped as

$$\sum_{l=0}^{\infty}\sum_{m=0}^{\infty}\sum_{n=0}^{\infty}a_{lmn}\phi_{lmn}\left(\boldsymbol{x}\right)=\sum_{\mu=0}^{\infty}\sum_{\nu=0}^{\infty}b_{\mu\nu}\varphi_{\mu\nu}\left(\boldsymbol{x}\right)\,. \tag{17}$$

Multiplying both sides of Eq. (17) by $\chi_{\mu'\nu'}$ and integrating over the opening yields

$$\begin{aligned}&\sum_{l=0}^{\infty}\sum_{m=0}^{\infty}\sum_{n=0}^{\infty}a_{lmn}\delta_{l,\mu'}\delta_{m,\nu'}\psi_n(0)\\&=i\rho kc\sum_{\mu=0}^{\infty}\sum_{\nu=0}^{\infty}b_{\mu\nu}\int_{S_{op}}\int_{S_{op}}\chi_{\mu'\nu'}G\chi_{\mu\nu}ds_{op}ds_{op}\end{aligned}. \tag{18}$$

Here, $Z_{\mu\nu,\mu'\nu'}=i\rho kc\sum_{\mu=0}^{\infty}\sum_{\nu=0}^{\infty}\int_{S_{op}}\int_{S_{op}}\chi_{\mu'\nu'}G\chi_{\mu\nu}ds_{op}ds_{op}$ is defined as the (modal) radiation impedance of the opening [42] such that Eq. (18) can be rewritten as

$$\sum_{l=0}^{\infty}\sum_{m=0}^{\infty}\sum_{n=0}^{\infty}a_{lmn}\delta_{l,\mu'}\delta_{m,\nu'}\psi_n(0)=\sum_{\mu=0}^{\infty}\sum_{\nu=0}^{\infty}b_{\mu\nu}Z_{\mu\nu,\mu'\nu'}. \tag{19}$$

Finally, the linear system can be obtained by combining Eqs. (15) and (19), which can be described in the matrix form as

$$\begin{bmatrix}\mathbf{K} & \mathbf{M}\\ \mathbf{\Phi} & \mathbf{Z}\end{bmatrix}\begin{bmatrix}\mathbf{A}\\ \mathbf{B}\end{bmatrix}=\begin{bmatrix}\mathbf{S}\\ \mathbf{0}\end{bmatrix}, \tag{20}$$

in which

$$\mathbf{A}=\{\cdots,a_{lmn},\cdots\}^T;\mathbf{B}=\{\cdots,b_{\mu\nu},\cdots\}^T, \tag{21}$$

$$\mathbf{K}=\begin{bmatrix}k^2-k_{000}^2,0,\cdots,0\\ 0,k^2-k_{010}^2,\cdots,0\\ \ddots\\ 0,0,\cdots,k^2-k_{lmn}^2\end{bmatrix}-i\rho kc\begin{bmatrix}\cdots,\phi_{000}(\boldsymbol{x}_t^R)/Z_t^R,\cdots\\ \cdots,\phi_{010}(\boldsymbol{x}_t^R)/Z_t^R,\cdots\\ \ddots\\ \cdots,\phi_{lmn}(\boldsymbol{x}_t^R)/Z_t^R,\cdots\end{bmatrix}\begin{bmatrix}\phi_{000}(\boldsymbol{x}_1^R),\phi_{010}(\boldsymbol{x}_1^R),\cdots,\phi_{lmn}(\boldsymbol{x}_1^R)\\ \phi_{000}(\boldsymbol{x}_2^R),\phi_{010}(\boldsymbol{x}_2^R),\cdots,\phi_{lmn}(\boldsymbol{x}_2^R)\\ \ddots\\ \phi_{000}(\boldsymbol{x}_T^R),\phi_{010}(\boldsymbol{x}_T^R),\cdots,\phi_{lmn}(\boldsymbol{x}_T^R)\end{bmatrix}, \tag{22}$$

$$\mathbf{M}=-i\rho kc\begin{bmatrix}\delta_{0,0}\delta_{0,0}\psi_0(0), & \delta_{0,0}\delta_{0,1}\psi_0(0), & \cdots, & \delta_{0,\mu}\delta_{0,\nu}\psi_0(0)\\ \delta_{0,0}\delta_{1,0}\psi_0(0), & \delta_{0,0}\delta_{1,1}\psi_0(0), & \cdots, & \delta_{0,\mu}\delta_{0,\nu}\psi_0(0)\\ & \ddots & & \\ \delta_{l,0}\delta_{m,0}\psi_n(0), & \delta_{l,0}\delta_{m,1}\psi_n(0), & \cdots, & \delta_{l,\mu}\delta_{m,\nu}\psi_n(0)\end{bmatrix}, \tag{23}$$

$$\mathbf{\Phi}=\begin{bmatrix}\delta_{0,0}\delta_{0,0}\psi_0(0), & \delta_{0,0}\delta_{1,0}\psi_0(0), & \cdots, & \delta_{l,0}\delta_{m,0}\psi_n(0)\\ \delta_{0,0}\delta_{0,1}\psi_0(0), & \delta_{0,0}\delta_{1,1}\psi_0(0), & \cdots, & \delta_{l,0}\delta_{m,1}\psi_n(0)\\ & \ddots & & \\ \delta_{0,l}\delta_{0,m}\psi_0(0), & \delta_{0,l}\delta_{1,m}\psi_0(0), & \cdots, & \delta_{l,l}\delta_{m,m}\psi_n(0)\end{bmatrix}, \tag{24}$$

$$\mathbf{Z}=\begin{bmatrix}Z_{00,00},Z_{00,01},\cdots,Z_{00,\mu\nu}\\ Z_{01,00},Z_{01,01},\cdots,Z_{01,\mu\nu}\\ \ddots\\ Z_{\mu\nu,00},Z_{\mu\nu,01},\cdots,Z_{\mu\nu,\mu\nu}\end{bmatrix}, \tag{25}$$

$$\mathbf{S} = -i\rho kcq_s \left\{ \cdots, \phi_{lmn}\left(\boldsymbol{x}_s\right), \cdots \right\}^T . \tag{26}$$

The maximum number of eigenfunctions used in Eqs. (6) and (10) are truncated to $\boldsymbol{N}$ and $\boldsymbol{M}$, respectively, following the same procedure as in Pierce [41], which is not reported herein as it has appeared frequently in the literature. The coefficient vectors $\mathbf{A}$ and $\mathbf{B}$ can be obtained by solving Eq. (20). Therefore, the sound field inside and outside the cavity can also be evaluated based on Eqs. (6) and (11).

3. Theoretical results and discussions

3.1 Model validation

In this section, numerical simulations are investigated to examine the accuracy of the theoretical model proposed in Section 2. The rectangular open cavity described in the current study is of dimensions L_x = 0.7 m, L_y = 0.48 m, and L_z = 0.54 m. The sound speed in air is c = 340 m/s, and the density of air is ρ = 1.225 kg/m^3. The source is located at (0.05, 0.085, -0.49) m while the receivers are randomly selected at (0.45, 0.085, -0.05) m and (1.5, 1.28, 1) m, and denoted as R1 and R2, respectively.

Modal truncation was performed first by evaluating the convergence in the frequency range of [50 Hz, 500 Hz]. The amplitude and phase of the sound pressure at the abovementioned receivers were evaluated as the modal number increases. For the acoustic cavity modes ϕ_{lmn} used in Eq. (6), the total number was truncated to $\boldsymbol{N}$ = 300 while that of $\chi_{\mu\nu}$ in Eq.(10) was truncated to $\boldsymbol{M}$ = 40. The calculated results indicate that 300 cavity modes and 40 external modes are sufficient, as a further increase in the numbers renders no significant difference.

To validate the proposed theoretical model, the sound fields inside and outside the open cavity are compared with the numerical results calculated using the BEM. The maximum size of the constant elements in the BEM simulation was 0.02 m, in which at least 30 elements per wavelength were used to ensure a higher accuracy. Figures 2(a) and 2(b) show the comparison of the sound pressure level

(SPL) spectrum obtained by the proposed theoretical method and BEM at receiver R1 inside the cavity and R2 outside the cavity, respectively. It is revealed that the results obtained by the proposed theory agree well with the numerical results of the BEM, which fully support the accuracy of the model established. According to the comparison above, the proposed theoretical approach is validated and will be used to predict the acoustical coupling of the open cavity and resonator in the following studies.

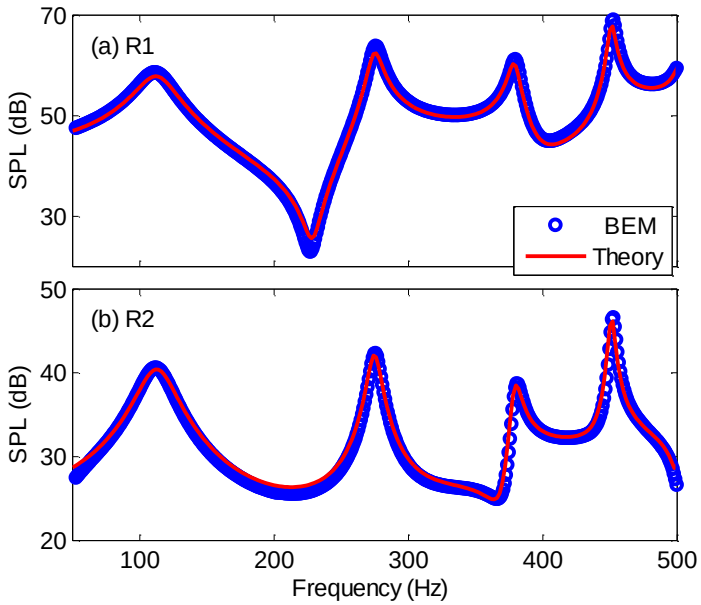

Figure 2 Comparison of sound pressure levels at receivers between the proposed theory and the BEM.

3.2 Noise radiation suppression by inserting a single resonator

An HR was designed accordingly to suppress the second sound peak, as shown in Figure 3. When the HR is mounted on the cavity wall, an acoustical interaction occurs between the open cavity and resonator. The sound pressure spectrum in the two spaces Ω_a and Ω_b is therefore changed significantly. Herein, the resonator is named HR with a number representing the natural frequency of the resonator. As shown in Figure 3, a typical sound peak can be found at 274 Hz for both receivers. To reduce the acoustical response at this frequency, HR272 was designed and was located at (0, 0.05, -0.49) m. The resonator used in the current study is illustrated in Figure 1, which consists of a short neck branch and long body branch. The physical parameters of HR272 will be described in detail in Section 4.1. The output impedance at the aperture of such a resonator can be calculated based on the method proposed

in Ref. [35].

Figure 3 depicts the SPL at the receiving point R2 for the open cavity with and without HR272. As illustrated in Figure 3, the SPLs around the target peak of 274 Hz are suppressed significantly using HR272 and reduced from 42.05 dB to 28.62 dB at 274 Hz. Furthermore, noise reduction is observed primarily within the frequency range of approximately 262 Hz and 289 Hz. Using the resonator, two peaks of relatively low sound pressure level at the frequencies of 256 Hz and 283 Hz instead of the original peak with a high amplitude are observed.

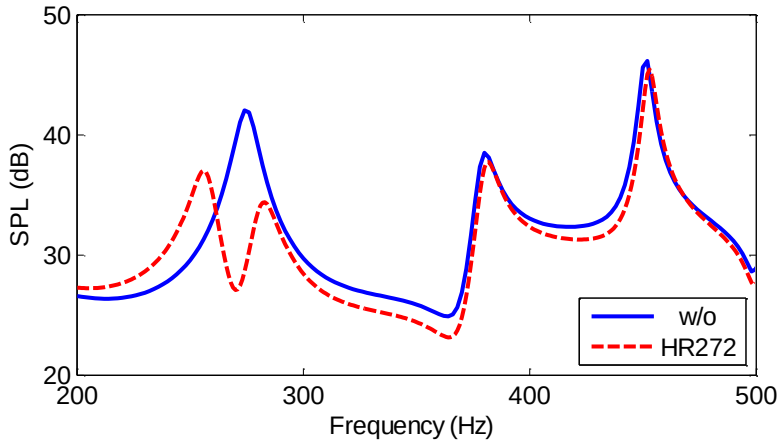

Figure 3 Comparison of sound pressure level at receiving point R2 for the open cavity with and without HR272.

To explain this phenomenon, an eigenvalue analysis of the acoustical open cavity coupled with and without the resonator was performed here. In the absence of the primary sound source, i.e. $q_s = 0$, Eq. (15) will be simplified into the following form:

$$\begin{aligned} &a_{lmn}\left(k^2-k_{lmn}^2\right)-i\rho kc\sum_{\mu=0}^{\infty}\sum_{\nu=0}^{\infty}b_{\mu\nu}\int_{S_{op}}\phi_{lmn}\chi_{\mu\nu}ds_{op} \\ &=\frac{i\rho kc}{Z_1^R}\phi_{lmn}\left(\boldsymbol{x}^R\right)\sum_{l'=0}^{\infty}\sum_{m'=0}^{\infty}\sum_{n'=0}^{\infty}a_{l'm'n'}\phi_{l'm'n'}\left(\boldsymbol{x}^R\right) \end{aligned}. \tag{27}$$

Using Eqs. (20) and (27), the characteristic matrix equation for the open cavity coupled with a single resonator is written as

$$\begin{bmatrix} \mathbf{K} & \mathbf{M} \\ \mathbf{\Phi} & \mathbf{Z} \end{bmatrix}\begin{bmatrix} \mathbf{A} \\ \mathbf{B} \end{bmatrix}=\begin{bmatrix} \mathbf{0} \\ \mathbf{0} \end{bmatrix}. \tag{28}$$

The eigensolutions of the coupled system can subsequently be obtained by nullifying the

determinant of the matrix $\begin{bmatrix} \mathbf{K} & \mathbf{M} \\ \mathbf{\Phi} & \mathbf{Z} \end{bmatrix}$.

The eigensolutions are shown in Table 1. The first column lists the number of sound peaks observed at R2 in the frequency range from 50 to 500 Hz, while the second column presents the frequencies of the corresponding peaks. The following two columns are the modal indices and resonances of the enclosed cavity, which contributed primarily to the sound peaks. The left parts in Table 1 are the eigenfrequencies of the trapped mode for the open cavity without a resonator (f_{tm}) and that with a resonator (f_{tm}^{HR}). As shown in Table 1, relative to the eigenvalues characterised by the real spectra for the closed cavity, open systems exhibit a complex form that includes a real and imaginary part. For example, the eigenfrequency corresponding to an enclosed cavity mode (010) is 242.9 Hz, whereas the eigenvalue for the baffled open cavity is (272.6 + 4.4i). The imaginary part in the eigenfrequency indicates the radiation loss in the semi-infinite space Ω_b. Additionally, the real part of the eigensolutions for an open acoustical system is shifted slightly to a higher value when compared to the closed counterpart. When resonator HR272 is mounted on the cavity wall and coupled to the acoustic mode of the open cavity, two new resonances appear at 252.6 + 0.9i and 278.6 + 3.9i, and they emerge and replace the original eigenfrequency (272.6 + 4.4i).

Table 1 Eigenfrequencies of the open cavity with and without resonator.

SPL at R2 w/o HR272		Enclosed-cavity		Trapped mode of open cavity w/o resonator	Trapped mode of open cavity with a HR272
peaks	f_{sp}	modal indices (lmn)	f_{cm}	f_{tm}	f_{tm}^{HR}
1	113	(000)	0	110.4+21.8i	110.4+21.8i
2	274	(100)	242.9	272.6+4.4i	252.6+0.9i
					278.6+3.9i
3	380	(010)	354.2	377.3+3.8i	378.3+3.9i
4	451	(110)	429.4	449.5+2.3i	450.9+2.4i

As shown in Figure 3, the SPL at receiver R2 after the open cavity integrated with the HR272 validates these two new resonances. A similar phenomenon has been investigated for an enclosure coupled with a single resonator [34, 35]. The amplitudes of these two new SPL peaks are influenced

by the location and internal resistance of the resonator, as well as the resonator's natural frequency. As the resonator used in this study is expected to control the noise radiation in a broad frequency band, these coupled peaks will be discussed in detail [36].

4. Noise radiation control strategy using Helmholtz resonators

As shown in Figure 2, four peaks at 113 Hz, 274 Hz, 380 Hz, and 451 Hz are observed, and the latter three peaks are close to the resonance frequency of the trapped mode of the open cavity. Figures 4(a), (b), and (c) show the sound pressure level distributions at 113 Hz, 274 Hz, and 380 Hz, respectively. Three slices that are parallel with the *x*-*y* plane at $z = z_s$, parallel with the *x*-*z* plane at $y = L_y/2$, and parallel with the *y*-*z* plane at $x = L_x/2$, were used to display the SPL distribution within the cavity space. The acoustic modal pattern caused by the four rigid walls of the rectangular cavity can be observed inside the open cavity at 274 Hz and 380 Hz. Meanwhile, the sound pressure level distribution at 113 Hz remains almost the same at the surface parallel to the *x*-*y* plane but varies vertically within the open cavity. As claimed by Wang et al. [2], the sound peak at 113 Hz is primarily due to the reflection from the bottom.

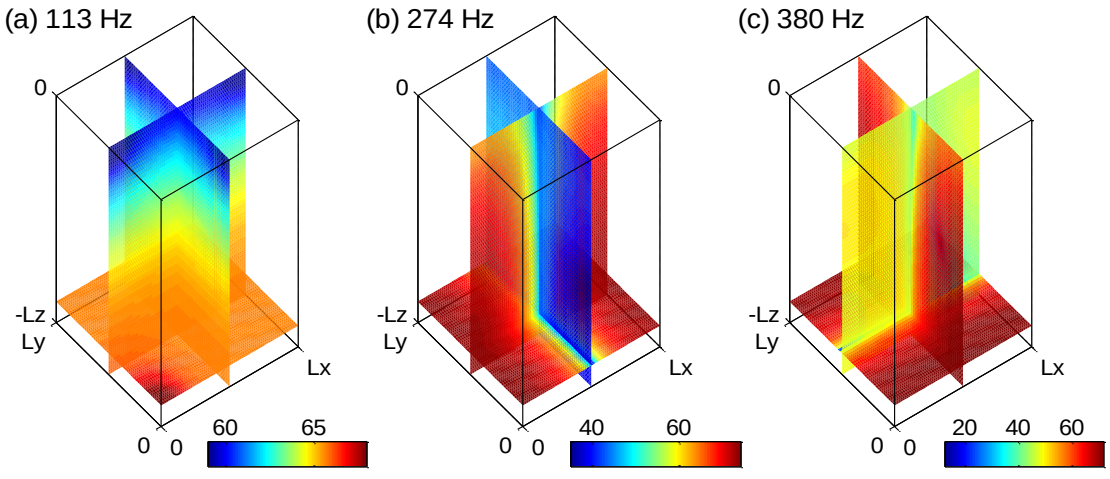

Figure 4 Sound pressure level distributions inside the baffled open cavity: (a) f = 113 Hz; (b) f = 274 Hz and (c) f = 380 Hz.

Figure 5 illustrates the amplitudes of modal coefficients a_{lmn} and $b_{\mu\nu}$ for the open cavity without a resonator. As indicated by Figures 5 (2a) and (2b), at 274 Hz, the acoustic response inside the open

cavity is dominated by the (100) enclosed-cavity mode, and that outside the open cavity is primarily contributed by the (10) external mode. Figures 5(3a) and (3b) show that the dominant enclosed-cavity mode and external mode at 380 Hz are (110) and (11), respectively. In this regard, if the dominant modal response is suppressed, the sound pressure radiation may be attenuated accordingly. Therefore, the noise control strategy of the acoustic modal-control-based approach is introduced to suppress the peak of the sound pressure level radiated from the open cavity.

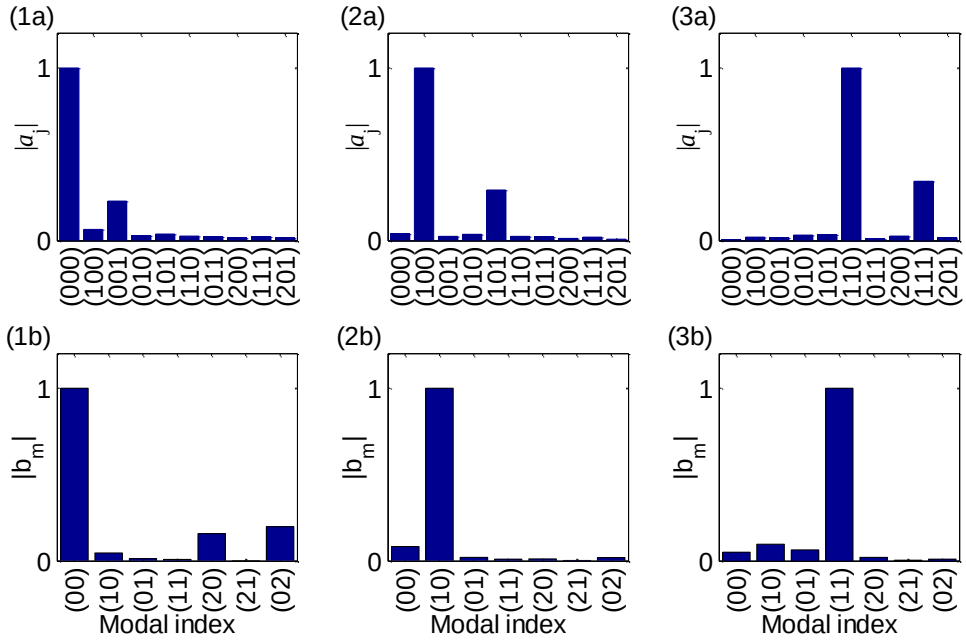

Figure 5 Model response for first ten enclosed-cavity modes and first seven external modes at three frequencies: (1a) $|a_j|$ at 113 Hz; (2a) $|a_j|$ at 274 Hz; (3a) $|a_j|$ at 380 Hz; (1b) $|b_m|$ at 113 Hz; (2b) $|b_m|$ at 274 Hz; (3b) $|b_m|$ at 380 Hz.

4.1 Noise radiation control using only one acoustical resonator

With reference to Eq. (15), apart from the acoustical coupling between the resonators and open cavity, acoustic interactions occur among the resonators. These interactions complicate the analysis of such an acoustical coupling system. To facilitate the exploration of the physics behind the interactions between the resonator and open cavity, one resonator instead of multiple resonators was adopted first. Therefore, the classical acoustical coupling problem between an open cavity and only one resonator was investigated using the proposed theoretical model.

Traditionally, the resonator is set on anti-nodal surfaces where the strongest acoustical coupling

occurs. This may result in the distortion of the acoustic modal response inside the open cavity and subsequently suppress the sound radiation effectively. Therefore, the sound response at the target frequency may be suppressed well. However, the noise response in the vicinity of the target frequency may be increased [36]. Therefore, the location of the single resonator should be optimised within a frequency band instead of only one peak frequency. Meanwhile, when the resonator location is fixed, the natural frequency and the internal resistance of the resonator, through the output impedance Z at the resonator aperture, are crucial in determining the noise reduction performance. Therefore, the Helmholtz frequency, and the location and internal resistance of the resonator must be investigated thoroughly.

4.1.1 Natural frequency of the Helmholtz resonator

When used in an acoustic enclosure [35, 43] the natural frequency of a resonator is tuned according to its modal resonance. However, to suppress the sound peak in an open acoustic system, for example the second peak at 274 Hz in the current study, three types of frequencies can be used to determine the natural frequency of the Helmholtz resonator: the resonant frequency of the enclosed cavity mode (100) f_{cm}, the resonant frequency of the open cavity trapped mode f_{tm}, and the frequency of the target sound peak f_{sp}. The values of these three frequencies are 242 Hz, 272 Hz, and 274 Hz, respectively. Therefore, to obtain a superior noise abatement around 274 Hz, the natural frequency of the HR should be determined first. Three resonators, denoted as HR242, HR272, and HR274 were used. They were designed to match the f_{cm} f_{tm}, and f_{sp}, respectively. The geometrical parameters for these three resonators are listed in Table 2. The radii of the circular neck branch and volume branch are indicated by r_1 and r_2, respectively. The physical lengths of these two branches are b_1 and b_2, respectively. These two resonators are mounted at the same position; subsequently, the sound responses at receiver R2 are compared.

Table 2 Geometrical parameters of the resonators HR242, HR272 and HR274.

Resonator	Resonant frequency [Hz]	Neck branch diameter r_1 [m]	Neck branch length b_1 [m]	Volume branch diameter r_2 [m]	Volume branch diameter b_2 [m]
HR242	242	0.02	0.0281	0.07	0.1
HR272	272	0.02	0.0196	0.07	0.1
HR274	274	0.02	0.0191	0.07	0.1

Figure 6 displays the resultant SPLs with and without resonators; it illustrates that the three types of resonators are effective in suppressing the target sound peak. The sound pressure level in the range of 237 Hz to 280 Hz is slightly reduced when HR242 is adopted, and the original peak at 274 Hz is reduced by approximately 3.9 dB. Meanwhile, noise reduction is shown clearly in the vicinity of the original sound peak when HR272 and HR274 are used, and the sound pressure levels at the peak are reduced by approximately 13.43 dB and 14.05 dB, respectively. The averaged noise reductions around 274 Hz with a bandwidth of 20 Hz are 2.66, 8.3, and 8.21 for HR242, HR272, and HR274, respectively. A better noise control performance around the original sound peak can be observed when the resonator is designed based on the open cavity trapped mode and the original sound peak.

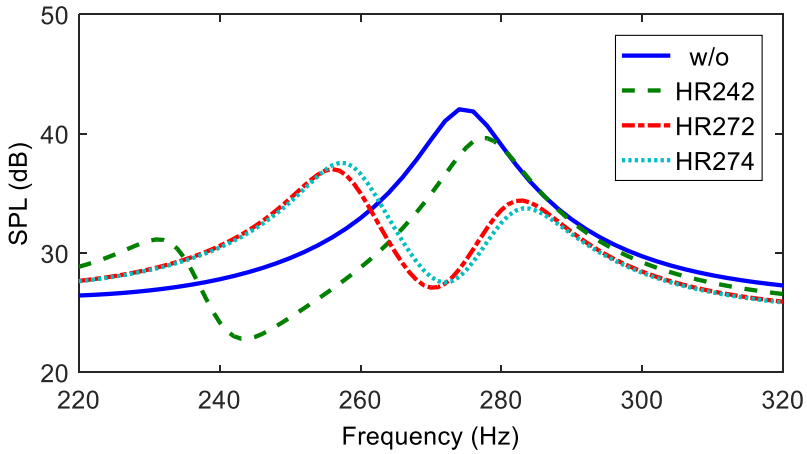

Figure 6 Sound pressure level variations when the natural frequency of the resonator tuned to three different values.

Shown in Figure 7 are the SPL contours on the cavity walls, and the baffled plane without and with the resonators HR242, HR272, and HR274, respectively. The changes in SPL distribution illustrate the effectiveness of using a single resonator to suppress the noise radiation from the open cavity. Figure 8(a) presents the modal amplitudes of the first 10 cavity modes; Figure 8(b) reveals the first six external

modes when the frequency of the primary source is 274 Hz. As shown in Figures 8(a) and (b), the second enclosed-cavity mode ϕ_{100} and the external mode φ_{10} are the primary contributors to the primary sound field inside and outside the open cavity, respectively. Controlled by the resonator, the second modes are still the primary contributor but their amplitudes attenuate significantly. The amplitude of the enclosed-cavity mode ϕ_{100} decreases by 36.5%, 79.1%, and 80.4% by the HR242, HR272, and HR274, respectively. To reduce the noise radiation from the cavity opening to the outside space, the natural frequency of the HR device should be designed based on the resonance of the trapped mode or the frequency of the original sound peak. It is observed that the noise reduction for a chosen bandwidth of 20 Hz centred at 274 Hz by HR272 is slightly higher than that by HR274. Therefore, the resonator HR272 was used subsequently.

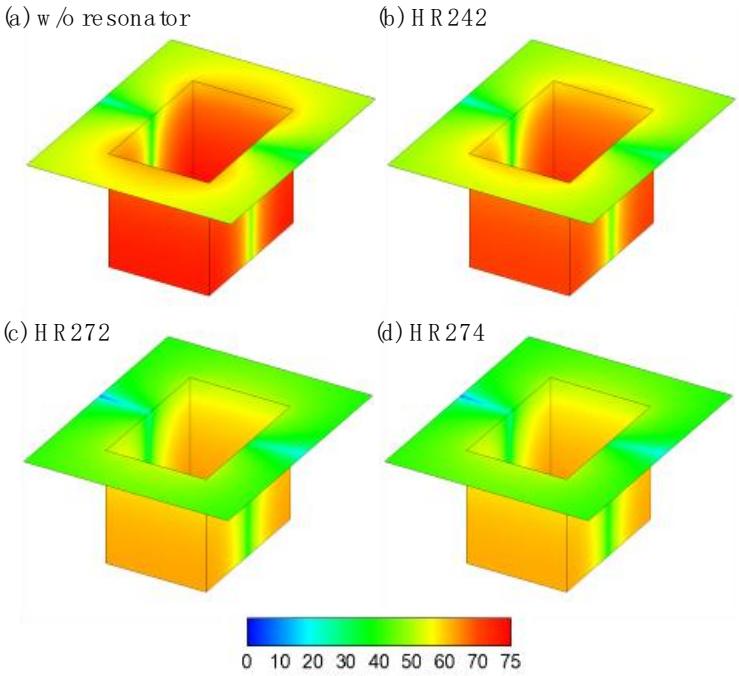

Figure 7 Sound pressure level distributions on the cavity walls and baffled plane at 274 Hz with and without one resonator: (a) without the resonator; (b) with HR242; (c) with HR272 and (d) with HR274.

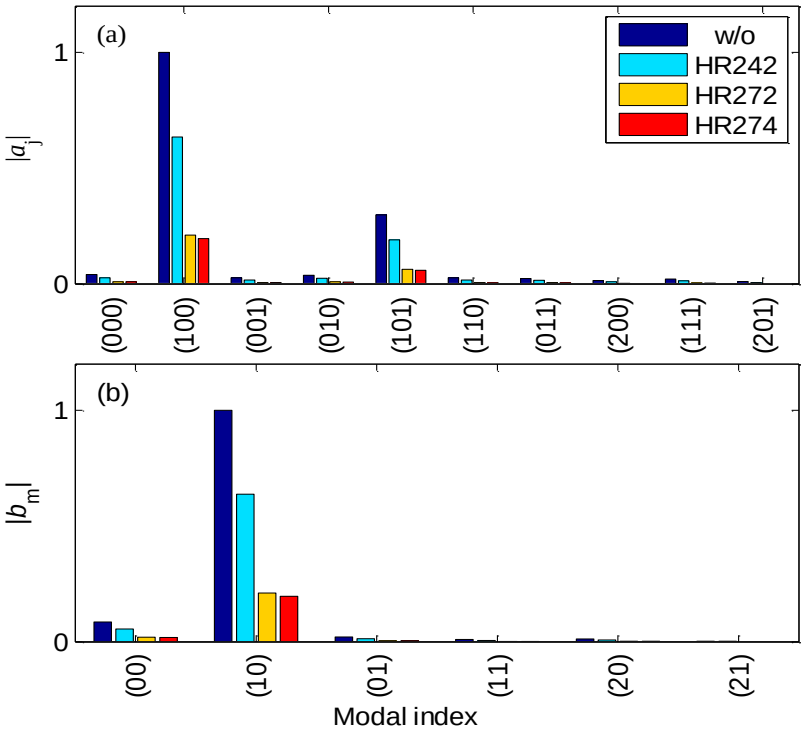

Figure 8 Model response for first ten enclosed-cavity modes and first seven external modes at 274 Hz with and without resonator: (a) $|a_j|$ at 274 Hz and (b) $|b_m|$ at 274 Hz.

4.1.2 Location of Helmholtz resonator

One HR272 is fixed at three different locations: M1 = (0.04, 0, -0.49) m, M2 = (0.7, 0.05, -0.49) m, and M3 = (0, 0.1, -0.44) m. Figure 9 illustrates the variation in SPL spectrum at receiver R2 when the HR272 is mounted at these positions. When the resonator is located at M1, which is close to the sound source, the noise level at 274 Hz is reduced by 11.85 dB. When the HR272 moved to M2 and M3, the noise reduction at the target sound peak is 5.67 dB and 11.39 dB, respectively. Generally, when a resonator is close to the anti-node region and near the primary sound source, the acoustical coupling between the cavity and resonator will be strong; hence, the noise reduction around the target frequency and its vicinity will be increased.

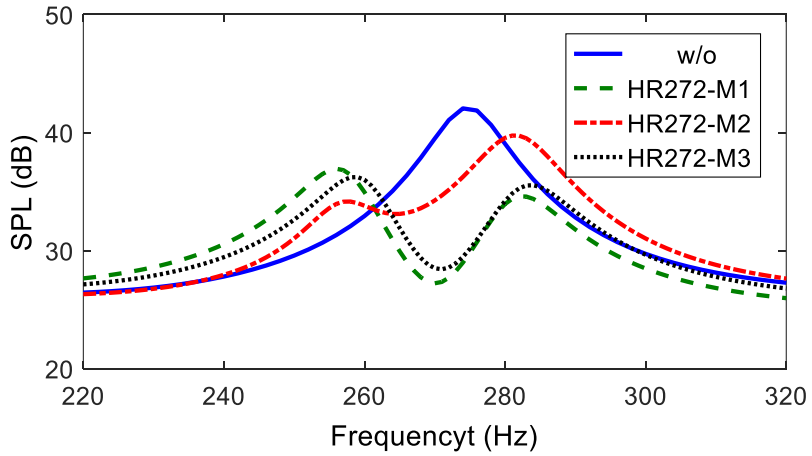

Figure 9 Sound pressure level variations at R2 when the same resonator are located at different positions.

The analysis above indicates that with different resonator positions, the noise reduction at the target frequency and its vicinity is different. In this regard, it is necessary to optimise the HR location to obtain a superior noise reduction. Owing to space limitation and practical application, the resonators were only mounted on the vertical surfaces of the cavity. A grid of step 10 mm in each direction was created for each surface; the frequency step is 1 Hz, and the SPL curves are computed for different HR locations at all grid points. After comparing with the SPLs for all locations, the SPL that provides the maximum SPL reduction in the vicinity of the targeted frequency is determined. Figure 10 shows the contour map of the averaged noise reduction at the receiving point R2 in the frequency range of 250 Hz and 300 Hz, as a function of the resonator location. Figure 10 (a), (b), (c), and (d) illustrate the result for the resonator mounted on the *x*-*z* plane at y = 0 m, *x*-*z* plane at $y = L_y$ m, *y*-*z* plane at x = 0 m, and *y*-*z* plane at $x = L_x$ m, respectively. The optimisation location for HR272 is found to be (0.04, 0, -0.48) m and the corresponding averaged SPL reduction is approximately 3.4 dB in that frequency range.

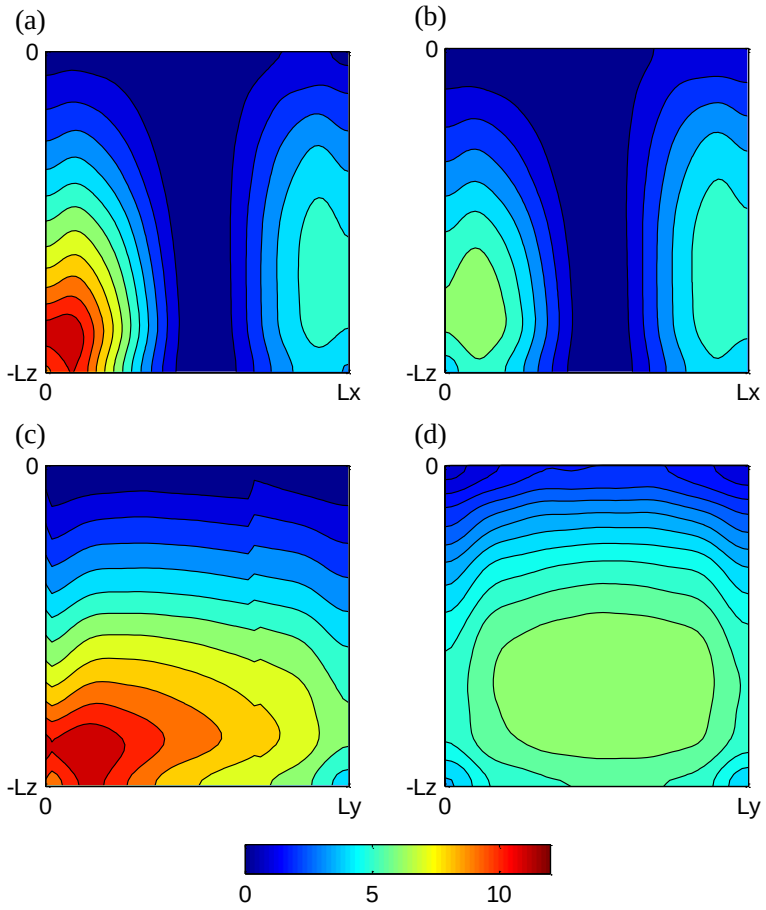

Figure 10 Averaged noise reductions in the selected frequency band when one HR272 is located at different positions of the cavity wall.

4.1.3 Internal resistance of Helmholtz resonator

The influence of internal resistance on suppressing the sound radiation from the open cavity is investigated in this section. The internal resistance of the resonator can be estimated by $R_i = \omega^R \rho L_{eff} / Q_R$, in which ω^R is the natural frequency of the resonator, L_{eff} is the effective length of resonator neck, and Q_R is the measured Q factor. In our study, three typical internal resistance values R_i are used and the resultant SPLs are compared in Figure 11. Two values of R_i = 2.25 and 9.62 mks Rayls are adopted from Yu et al. [37].

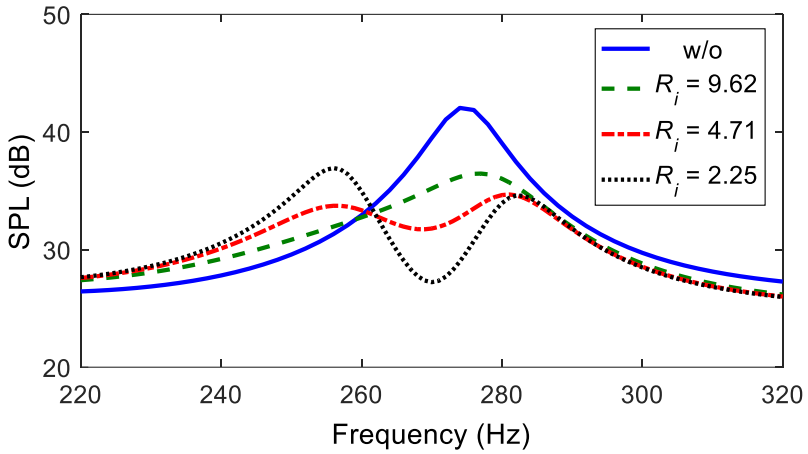

Figure 11 Sound pressure level variations at R2 when one HR272 with three different R_i.

As explained by the dashed line in Figure 11, a large internal resistance in the resonators improves the sound dissipation, but reduces the sound radiation from the resonators. Consequently, the acoustic interaction between the resonator and open cavity is weak. Therefore, an excessive internal resistance can only cause a moderate SPL reduction at the resonance peak. On the contrary, a low R_i in the resonators results in a significant SPL peak reduction at the resonator's natural frequency but at the expense of the appearance of two pronounced coupled peaks, which are indicated by a dotted line. In this case, most of the energy is radiated back to the cavity with little amount of energy dissipated by the resonator. This is attributed to the low mobility of the resonator aperture such that the resonator and the enclosure cannot be coupled effectively. None of the above scenarios is desirable. The demarcation and quantification of the effects of energy dissipation and radiation are crucial to understand how a resonator can be used with optimal internal resistance. When the resistance of the resonator is at approximately the optimal value (R_i = 4.71 mks Rayls in the current study, which is slightly higher than that used in [37]), the noise reduction is maximal and the peaks at the coupled frequencies are relatively flat, thus leading to a better overall sound reduction within the frequency band, as represented by dash-dotted line in Figure 11.

4.2 Multiple Helmholtz resonators on noise control

A resonator array consisting of resonators tuned with different natural frequencies can be adopted

to reduce the noise level at multiple sound peaks. The sound peaks may be excited by the primary sound source as well as the coupled sound peak by the insertion of the resonator. Based on the control achieved (as presented in Section 4.1), coupled peaks can be avoided if the resonator with optimised location and internal resistance is inserted. Moreover, the original sound peaks stimulated by the primary sound source deserve more attention. Therefore, the current study focuses on suppressing the sound peaks generated by the primary sound source. Three resonators: HR272, HR378, and HR449 were designed to suppress the sound pressure level peaks at 274, 380, and 452 Hz, respectively. The optimal location of these three resonators were obtained based on the averaged sound pressure level for a chosen frequency bandwidth of 20 Hz centred at 274 Hz, 380 Hz, and 452 Hz, respectively.

Table 3 Geometrical parameters and locations of the resonator HR272, HR378 and HR449.

Resonator	Resonant frequency [Hz]	Neck Branch diameter r_1 [m]	Neck Branch length b_1 [m]	Volume diameter r_2 [m]	Volume length b_2 [m]	Positions [m, m, m]
HR272	272	0.02	0.0196	0.07	0.1	(0.04, 0, -0.48)
HR378	378	0.015	0.0284	0.045	0.06	(0, 0.05, -0.49)
HR449	449	0.012	0.026	0.036	0.048	(0, 0.05, -0.44)

The geometric dimensions and optimal locations of these three resonators are listed in Table 3. The predicted SPL spectrum with and without the resonator array are shown in Figure 12. It is found that all three dominant peaks at 274 Hz, 380 Hz, and 452 Hz can be suppressed simultaneously, and results in noise reduction by 9.9 dB, 11.11 dB, and 16.58 dB, respectively. The averaged noise reduction in the frequency ranges of 264–284 Hz, 370–390 Hz, and 442–462 Hz are 5.26, 7.37, 9.27 dB, respectively. Therefore, significant wide band control can be achieved while avoiding the addition of more resonators.

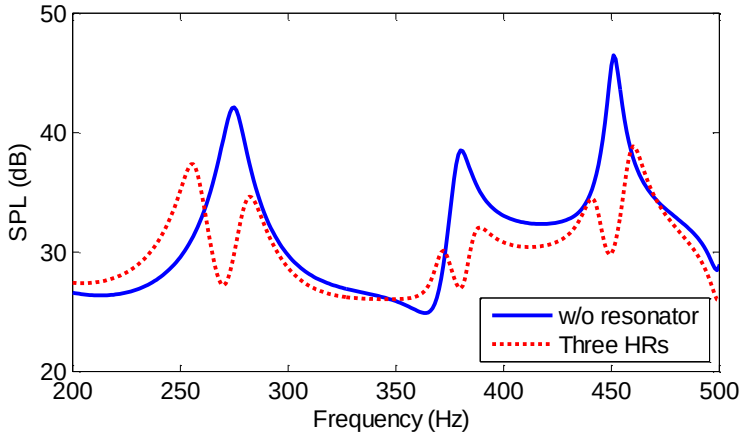

Figure 12 Sound pressure level variations at R2 after the cavity wall mounted with three resonators.

5. Experimental validation

Experiments were conducted to validate the theoretical result. Figure 13 is the sketch of the experimental setup in an anechoic chamber with an effective size of 6 m (length) ×6 m (width) ×4 m (height). The dimensions of the cavity used in the experiment were the same as that in the theoretical predictions. Two microphones (B&K type 4187) were positioned at R1 and R2, respectively. One was installed on the cavity walls and the other was supported by the tripod. Both AD (BNC 2120) and DA (NI 9234) converters were controlled by a LABVIEW program which is made to run within a range of testing frequencies from 200 to 500 Hz. The output noise signal from the DA converter was passed firstly via a power amplifier (LA 1201) and then to loudspeaker.

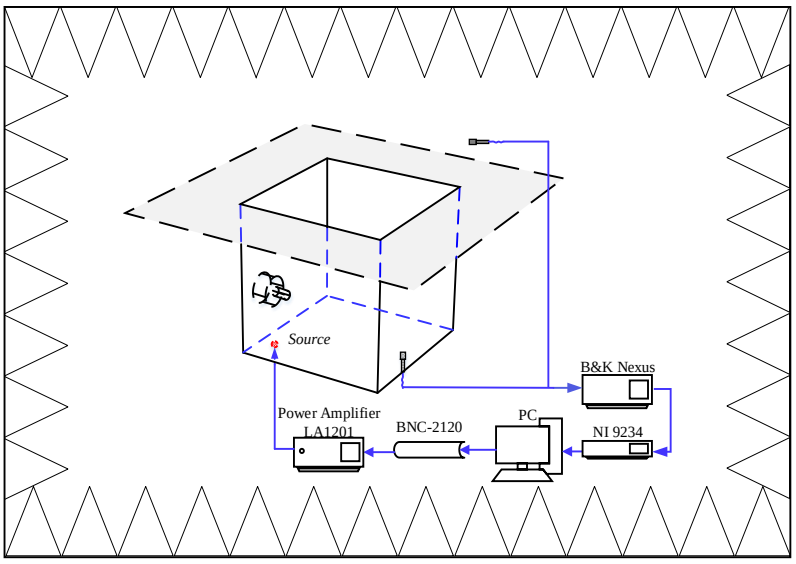

Figure 13 The schematic of the experimental setup.

(a)

(b)

(c)

Figure 14 Experimental photo for the baffled open cavity coupled with a resonator in anechoic chamber.

Figures 14 (a)-(c) illustrate the photos of the baffled open cavity integrated with an acoustic resonator used in experiment. The open cavity was constructed from five 20 mm-thick acrylic glass plates to approximate an ideal sound reflective material and prevent sound transmission through side walls. Shown in Figure 14(a) is the rectangular cavity opening, which has a same size as that in the theoretical calculations and was located at the center of the baffled panel. The baffle plane was made of plywood panels of thickness 18.5 mm, covered with a hard and smooth laminate. The primary source generated by a BMS 4599ND 2" Dual Diaphragm Driver loudspeaker was located at (0.05, 0.05, -0.49) m to excite the acoustical resonance inside the open cavity. The loudspeaker was installed outside the cavity and mounted in an aluminum tube of diameter 0.02 m to simulate a point source radiating into

the cavity, as shown in Figure 14(b). Three Helmholtz resonators, HR272, HR378 and HR449, were used in the experiment. Figure 14(c) illustrates the HR378 mounted on the cavity wall. The resonator HR272 was mounted at (0.05, 0, -0.49) m which was different from the optimized position. HR378 and HR449 were fixed at the locations according to the predicted results as shown in Table 3.

Practically, the frequency response of the loudspeaker is not always flat. Therefore, the loud speaker was regulated to equalisation first by inverse filtering. Subsequently, the sound amplitude emitted from the loudspeaker exhibited almost the same level (±0.3 dB) in the frequency range of interest [44].

To examine the accuracy of the proposed theoretical model, a comparison of the sound pressure level at the same receivers was performed. First, the sound pressure levels predicted by the proposed theoretical method and measured experimentally were compared for the baffled open cavity without the resonator. Figure 15 (a) shows the SPLs at (0.9, 0.88, 0.2) m outside the open cavity; a good agreement is found between the theoretical predictions (solid line) and experimental measurements (dashed line with circle), thus demonstrating that the proposed model can accurately predict the sound response outside the baffled open cavity.

Next, the comparison between theory and measurement for the baffled open cavity with resonator was performed. Figures 15 (b) and (c) show the performance of the open cavity with a single resonator and three resonators, respectively. In these figures, the theoretical predictions are presented by the solid line, while the measured data are indicated by the dashed line marked with circles. The agreement between the theoretical results and experimental data is relatively good. Using a single resonator, both theory and experiment indicate that the original SPL peak at 274 Hz is reduced significantly. Using three resonators (HR272, HR378, and HR449), the three target SPL peaks are reduced. The comparisons in Figure 15 show the accuracy of the proposed theoretical method for the acoustical coupling between the baffled open cavity and the single or multiple resonators, and validate the feasibility of using an HR for control sound radiation from open acoustic systems.

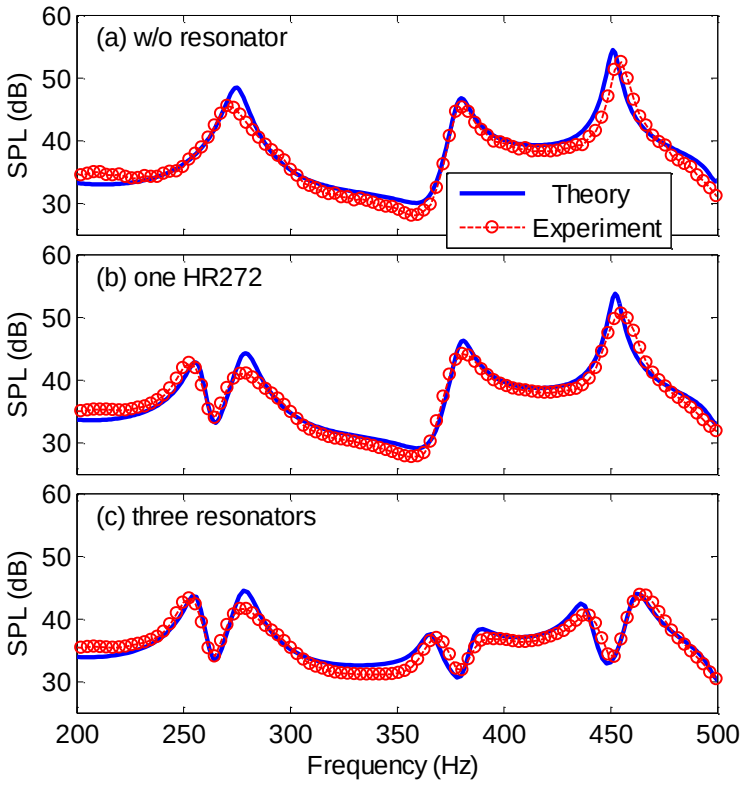

Figure 15 Measured and predicted sound pressure level comparisons at outside receiver with and without acoustic resonators. (a) baffled open cavity without resonator; (b) baffled open cavity with one HR272 and (c) baffled open cavity with three resonators, HR272, HR378 and HR449 .

6. Conclusions

This paper presents an approach to model the acoustical coupling of an open cavity and resonator array as well as the sound radiation control in an acoustical open cavity. A theoretical model for the acoustical coupling between a baffled open cavity and an array of HRs based on the modal coupling method was established. A general solution was obtained for predicting the sound pressure inside and outside the baffled open cavity with or without HRs. The accuracy of the proposed method was successfully verified by the BEM.

The theoretical analysis demonstrated that the sound peaks inside and outside the baffled open cavity were dominated by one cavity mode while contributed from other modes. The natural frequency, location, and internal resistance that determined the noise abatement performance of the resonator within a frequency band were investigated. The most desirable noise suppression of the spectrum peak could be achieved when the HR was designed with its natural frequency matching the resonance

frequency of the open cavity in the trapped mode. The coupling effect of the resonator with cavity space became weak as the resonator moved towards the cavity opening; consequently, the noise suppression at the outside receiver decreased. When the resistance of the resonator was close to the optimal value, the noise reduction was maximal and the peaks at the coupled frequencies were relatively flat, thus resulting in an overall sound reduction within the frequency band. Finally, the theoretical model was experimentally validated by measurements performed in an anechoic chamber. The feasibility of reducing noise radiation from an open cavity using HRs was confirmed.

Acknowledgement

The authors would like to acknowledge the funding support from The Research Grants Council of the Hong Kong SAR government (PolyU 5140/13E) and The Hong Kong Polytechnic University (G-YBN2) and (G-YBYA).

References

[1] C.K.W. Tam, The acoustic modes of a two-dimensional rectangular cavity, Journal of Sound and Vibration, 49 (1976) 353-364.

[2] S. Wang, J. Tao, X. Qiu, Performance of a planar virtual sound barrier at the baffled opening of a rectangular cavity, The Journal of the Acoustical Society of America, 138 (2015) 2836-2847.

[3] T. Pàmies, J. Romeu, M. Genescà, A. Balastegui, Sound radiation from an aperture in a rectangular enclosure under low modal conditions, The Journal of the Acoustical Society of America, 130 (2011) 239-248.

[4] Y.-H. Kim, S.-M. Kim, Solution of coupled acoustic problems: a partially opened cavity coupled with a membrane and a semi-infinite exterior field, Journal of sound and vibration, 254 (2002) 231-244.

[5] G. Jin, S. Shi, Z. Liu, Acoustic modeling of a three-dimensional rectangular opened enclosure coupled with a semi-infinite exterior field at the baffled opening, The Journal of the Acoustical Society of America, 140 (2016) 3675-3690.

[6] S. Shi, Z. Su, G. Jin, Z. Liu, Vibro-acoustic modeling and analysis of a coupled acoustic system comprising a partially opened cavity coupled with a flexible plate, Mechanical Systems and Signal Processing, 98 (2018) 324-343.

[7] C. Yang, J. Pan, L. Cheng, A mechanism study of sound wave-trapping barriers, The Journal of the Acoustical Society of America, 134 (2013) 1960-1969.

[8] F. Polonio, T. Loyau, J.-M. Parot, G. Gogu, Acoustic radiation of an open structure: Modeling and experiments, Acta Acustica united with Acustica, 90 (2004) 496-511.

[9] J. Zhenlin, M. Qiang, Z. Zhihua, Application of the boundary element method to predicting acoustic performance of expansion chamber mufflers with mean flow, Journal of Sound and Vibration, 173 (1994) 57-71.

[10] H.-L. Choi, D.J. Lee, Development of the numerical method for calculating sound radiation from a rotating dipole source in an opened thin duct, Journal of sound and vibration, 295 (2006) 739-752.

[11] A. Seybert, C. Cheng, T. Wu, The solution of coupled interior/exterior acoustic problems using the boundary element method, The Journal of the Acoustical Society of America, 88 (1990) 1612-1618.

[12] E. Quaranta, D. Drikakis, Noise radiation from a ducted rotor in a swirling-translating flow, Journal of Fluid Mechanics, 641 (2009) 463-473.

[13] W. Duan, R. Kirby, A hybrid finite element approach to modeling sound radiation from circular and rectangular ducts, The Journal of the Acoustical Society of America, 131 (2012) 3638-3649.

[14] Y. Tong, Y. Kou, J. Pan, Forced acoustical response of a cavity coupled with a semi-infinite space using coupled mode theory, Wave Motion, (2017).

[15] S. Félix, J.-B. Doc, M.A. Boucher, Modeling of the multimodal radiation from an open-ended waveguide, The Journal of the Acoustical Society of America, 143 (2018) 3520-3528.

[16] J.-P. Berenger, A perfectly matched layer for the absorption of electromagnetic waves, Journal of computational physics, 114 (1994) 185-200.

[17] C. Hazard, On the absence of trapped modes in locally perturbed open waveguides, IMA Journal of Applied Mathematics, 80 (2014) 1049-1062.

[18] D. Evans, C. Linton, Trapped modes in open channels, Journal of fluid mechanics, 225 (1991) 153-175.

[19] S. Hein, W. Koch, Acoustic resonances and trapped modes in pipes and tunnels, Journal of Fluid Mechanics, 605 (2008) 401-428.

[20] Y. Duan, W. Koch, C.M. Linton, M. McIVER, Complex resonances and trapped modes in ducted domains, Journal of Fluid Mechanics, 571 (2007) 119-147.

[21] S. Hein, W. Koch, L. Nannen, Trapped modes and Fano resonances in two-dimensional acoustical duct–cavity systems, Journal of fluid mechanics, 692 (2012) 257-287.

[22] W. Koch, Acoustic resonances in rectangular open cavities, AIAA journal, 43 (2005) 2342-2349.

[23] W. Koch, Acoustic resonances and trapped modes in annular plate cascades, Journal of Fluid Mechanics, 628 (2009) 155-180.

[24] L. Xiong, W. Bi, Y. Aurégan, Fano resonance scatterings in waveguides with impedance boundary conditions, The Journal of the Acoustical Society of America, 139 (2016) 764-772.

[25] S. Hein, T. Hohage, W. Koch, On resonances in open systems, Journal of Fluid Mechanics, 506 (2004) 255-284.

[26] S. Wang, J. Tao, X. Qiu, J. Pan, Mechanisms of active control of sound radiation from an opening with boundary installed secondary sources, The Journal of the Acoustical Society of America, 143 (2018) 3345-3351.

[27] S. Wang, J. Tao, X. Qiu, Controlling sound radiation through an opening with secondary loudspeakers along its boundaries, Scientific reports, 7 (2017) 13385.

[28] S. Wang, J. Yu, X. Qiu, M. Pawelczyk, A. Shaid, L. Wang, Active sound radiation control with secondary sources at the edge of the opening, Applied Acoustics, 117 (2017) 173-179.

[29] S. Ortiz, C. Gonzalez, P. Cobo, F. Montero de Espinosa, Attenuating open cavity tones by lining its walls with microperforated panels, Noise Control Engineering Journal, 62 (2014) 145-151.

[30] Z.B. Wang, Y.S. Choy, Tunable parallel barriers using Helmholtz resonator, Journal of Sound and Vibration, 443 (2019) 109-123.

[31] K. Chen, Y. Chen, K. Lin, C. Weng, The improvement on the transmission loss of a duct by adding Helmholtz resonators, Applied Acoustics, 54 (1998) 71-82.

[32] A. Selamet, V. Kothamasu, J. Novak, Insertion loss of a Helmholtz resonator in the intake system of internal combustion engines: an experimental and computational investigation, Applied Acoustics, 62 (2001) 381-409.

[33] S.-H. Seo, Y.-H. Kim, Silencer design by using array resonators for low-frequency band noise reduction, The Journal of the Acoustical Society of America, 118 (2005) 2332-2338.

[34] D. Li, L. Cheng, Acoustically coupled model of an enclosure and a Helmholtz resonator array, Journal of sound and vibration, 305 (2007) 272-288.

[35] D. Li, L. Cheng, G. Yu, J. Vipperman, Noise control in enclosures: Modeling and experiments with T-shaped acoustic resonators, the Journal of the Acoustical Society of America, 122 (2007) 2615-2625.

[36] G. Yu, L. Cheng, Location optimization of a long T-shaped acoustic resonator array in noise control of enclosures, Journal of Sound and Vibration, 328 (2009) 42-56.

[37] G. Yu, D. Li, L. Cheng, Effect of internal resistance of a Helmholtz resonator on acoustic energy reduction in enclosures, The Journal of the Acoustical Society of America, 124 (2008) 3534-3543.

[38] F.-M. Dittes, The decay of quantum systems with a small number of open channels, Physics Reports, 339 (2000) 215-316.

[39] K. Pichugin, H. Schanz, P. Šeba, Effective coupling for open billiards, Physical Review E, 64 (2001) 056227.

[40] A. Lyapina, D. Maksimov, A. Pilipchuk, A. Sadreev, Bound states in the continuum in open acoustic resonators, Journal of Fluid Mechanics, 780 (2015) 370-387.

[41] A.D. Pierce, Acoustics: an introduction to its physical principles and applications, McGraw-Hill New York, 1981, pp. 213-215.

[42] F.J. Fahy, Foundations of engineering acoustics, Academic press, 2000.

[43] F. Fahy, C. Schofield, A note on the interaction between a Helmholtz resonator and an acoustic mode of an enclosure, Journal of Sound and Vibration, 72 (1980) 365-378.

[44] S. Ortiz, L. González, C.G. Díaz, U. Svensson, P. Cobo, Acoustic resonances in a 3D open cavity with non-parallel walls, Journal of Sound and Vibration, 363 (2016) 181-198.

Figure and table captions